Propagation Velocity Model of Stress Wave in Longitudinal Section of Tree in Different Angular Directions

Xiwen Wei,[a,b] Liping Sun,[a,]* Quansheng Sun,[a,]* Shuzheng Xu,[a] Hongjv Zhou,[a] and Chunxiao Du [c]

In order to detect the size and shape of defects inside wood, a propagation velocity model of stress wave in the longitudinal section of trees in different direction angles was proposed and evaluated. The propagation velocity model was established through theoretical analysis. Four representative tree species in the northeast region of China were taken as test samples. The propagation velocity of stress wave in the longitudinal section of trees in different directions was measured using a nondestructive testing instrument. The corresponding regression model was obtained, which was in good agreement with the theoretical mathematical model. For the larch log samples, a healthy multiple regression model ($z = 109.2x^2 - 182.1y^2 + 36.78x^2y^2 - 34.76x^2y^4 + 1627$) with correlation coefficient $R^2 = 0.97$ and root mean square error RMSE =17.81 was used to conduct two-dimensional imaging of defective logs. Based on the results of two-dimensional imaging, the highest fitness of the images was 94.24%, and the lowest error rates of defect cavities was 6.11%. The imaging results showed that this method accurately detected the internal defects of trees and was not affected by the size of defects.

Keywords: Stress wave nondestructive testing; Trees; Direction angle; Longitudinal Section; Two-dimensional imaging

*Contact information: a: College of Mechanical and Electrical Engineering, Northeast Forestry University, Harbin, 150040, China; b: Department of electrical and Information Engineering, Heilongjiang University of Technology, Jixi, 158100, China; c: Harbin Veterinary Research Institute, Chinese Academy of Agricultural Sciences, Harbin, 150040, China; *Corresponding author: zdhslp@163.com; hrbsqs@126.com*

INTRODUCTION

Internal defects such as decay and voids affect the physical and mechanical properties of wood, reduce the quality of wood, and affect its value. Therefore, rapid and accurate detection of wood to ascertain decay and internal defects improves the utilization rate of wood (Bucur 2005; Xu *et al.* 2018; Simic *et al*. 2019). Nondestructive testing technology does not destroy the properties and surface stability of testing samples. The application of non-destructive testing technology in wood detection has been well developed (Wang *et al.* 2001; Watanabe *et al.* 2008).

Stress wave detection technology can detect the mechanical properties and internal defects of wood. It is the most applicable and widely used non-destructive testing technology for wood (Yang and Wang 2005). The basic principle is to use a pulse hammer to strike the transmitter sensor on the tested wood, so that the mechanical stress wave is generated inside the wood under stress. The propagation time of the stress wave from the transmitting end to the receiving end is measured and translated into the propagation velocity in the corresponding direction. The physical and mechanical properties and internal defects of wood are determined by analyzing the variation of stress wave propagation time and velocity (Liao *et al.* 2017). Stress wave imaging technology is used to analyze and understand the propagation law of stress wave in wood, collect the original propagation time and velocity data, and use the appropriate mathematical function model or spatial interpolation method to reconstruct the internal conditions by image (Feng *et al.* 2014; Du *et al.* 2015, 2018a). By using image processing technology to detect the location, size, and decay defects in wood, the internal situation of wood section can be visually reflected (Lin *et al.* 2011; Liang and Fu 2014; Du *et al*. 2018b). Compared with other wood non-destructive testing technologies, stress wave detection has strong anti-interference ability, long transmission distance, and no need for use of a coupling agent. The testing equipment is convenient to carry and harmless to human beings. It can detect defects of arbitrary volume and shape. There are many current reports on the non-destructive testing of wood by stress wave methods (Ross *et al.* 1998; Rabe *et al.* 2004; Liang and Fu 2012; Chang *et al.* 2016; Yue *et al.* 2019).

This paper explores the propagation law of stress waves in different angular directions and longitudinal section angles of healthy trees as the foundation of the physical and mechanical properties of wood. A theoretical model of stress wave propagation velocity was obtained for the longitudinal section of trees in different angles, and the accuracy of the theoretical model was verified through experiments. Based on the theoretical calculation and experimental verification of the larch (*Larix gmelinii*) log multiple regression model for fault imaging, high-precision two-dimensional images of different defect sizes were established. The defect areas in the two-dimensional space of the larch logs were clearly defined to accurately reflect the internal defects of the wood. This paper provides a new theory for quantitative characterization of internal defect decay and tree internal defects of larch vigorous wood.

Theory of Stress Wave Propagation in Longitudinal Section of Tree in Different Direction Angles

Wood is an orthogonal material with mechanical and thermal properties that are single-valued and independent in the direction of three mutually perpendicular principal axes (Romano *et al.* 2008). For the sake of simplicity, assuming that an ideal wood piece is a cylinder, a three-dimensional coordinate system of wood with *O* as the origin is established as shown in Fig. 1(a), where *OL* represents the longitudinal axis and is parallel to the grain direction; *OR* represents the radial axis, perpendicular to the growth ring; and *OT* represents the tangent axis, tangent to the growth ring. It is further assumed that the stress wave propagates in the *OS* direction in the radial axis section, *O* represents the position of the stress wave emitting end sensor, *S* represents the position of the stress wave receiving end sensor, and α represents the angle between the *OR* and the *OS*, *i.e.*, the angle between the radial direction and the propagation direction of the stress wave. In addition, its cross section is considered as a regular circle. As shown in Fig. 1 (b), *O* represents the position of the sensor at the transmitter of stress wave, R_1 and R_2 represent the position of the sensor at the receiver of stress wave. The stress wave propagates in the direction of OR_1 and OR_2. The angle between them is expressed by β. The propagation velocity in the OR_1 direction is the radial propagation velocity, and the propagation velocity in the other directions is called the chord propagation velocity. Generally, the tensile strength in the longitudinal direction in healthy trees is higher, and the tensile strength in the radial and tangential directions is lower. The radial propagation velocity is the fastest, and the propagation velocity becomes slower as the chord angle increases (Wang *et al.* 2011; Liu and Li 2018).

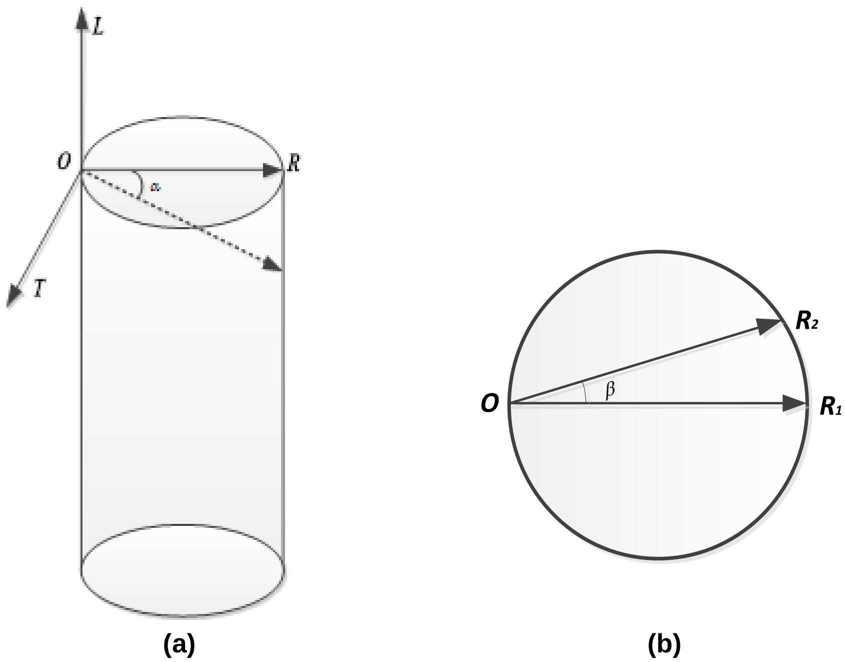

Fig. 1. Schematic diagram of (a) three-dimensional coordinate system of wood, (b) stress wave propagation in cross section

In practical applications, the force direction of the wood may be different from the direction of the wood grain formed naturally. In this case, the bearing capacity of the wood twill should to be considered. According to the twill compressive strength formula of wood summarized through a large number of experiments (Mascia *et al.* 2011), the formula for the propagation velocity of the stress wave on the direction angle can be derived as follows,

$$v(\alpha) = \frac{v_l v_r}{v_l \cos^2 \alpha + v_r \sin^2 \alpha} \tag{1}$$

where v_l represents the propagation velocity of stress wave in longitudinal section, v_r represents the propagation velocity of stress wave in radial axial.

If there is $\alpha = \frac{\pi}{2}$, then there is $v(\alpha) = v_l$,; if $\alpha = 0$, then there is $v(\alpha) = v_r$. The second-order Taylor expansion formula (Eq. 1) is used at $\alpha = 0$, and the remainder is removed to obtain the following formula,

$$v(\alpha) \approx v_r + v_r (1 - \frac{v_r}{v_l}) \alpha^2 \tag{2}$$

where v_l and v_r are determined by the nature of wood itself, so the relationship between the propagation velocity of stress wave and the direction angle is approximately an open parabola. Equation 2 is used as a theoretical model for the propagation of stress waves in healthy trees in different directions.

The acoustic anisotropy of the wet material was analyzed experimentally according to Weng *et al.* (2016). The formula of the propagation velocity of the stress wave at the chord angle is obtained as follows,

$$v(\beta) \approx (1-0.2\beta^2)v_R \tag{3}$$

where the radial velocity when the angle of the section is 0 is expressed by v_R.

Equation 3 is used as a theoretical model for the propagation of stress waves in the angles of different longitudinal sections in healthy trees, which approximates a parabola with an opening downward.

By substituting Eq. 3 into Eq. 2, the propagation velocity $v(\alpha, \beta)$ of stress wave in longitudinal section with different directions is obtained as follows,

$$v(\alpha,\beta) = A\alpha^2 - B\beta^2 + C\alpha^2\beta^2 - D\alpha^2\beta^4 + K \tag{4}$$

where, $A = V_R - \frac{V_R^2}{V_l}$, $B = 0.2V_R$, $C = \frac{0.4V_R^2}{V_l} - 0.2V_R$, $D = \frac{0.04V_R^2}{V_l}$, $K = V_R$.

Equation 4 is a comprehensive theoretical mathematical model of stress wave propagation velocity and direction angle and section angle in healthy trees, it can be seen that the propagation velocity model of stress wave in longitudinal section with different directions is the sum of polynomials of direction angle and section angle.

EXPERIMENTAL

Materials and Equipment

The internal structure of trees is complex, and it is divided into radial, tangential and longitudinal directions. The propagation velocity of stress waves detected at different positions is very different (Huan *et al.* 2018). Therefore, tree samples were selected from representative non-node, non-decay, non-cracking, straight trunk of birch (*Betula platyphylla*), ashtree (*Fraxinus mandshurica*), elm (*Ulmus pumila*), and larch (*Larix gmelinii*) logs in Northeast China as test objects in order to avoid test errors. To ensure the theory that stress waves propagate on the vertical section of logs, the numbers of birch, ashtree, elm, and larch logs were counted as Y1, Y2, Y3, and Y4, respectively. The diameter at breast height (DBH) and height of healthy log samples were measured by a leather tape measure and a caliper. The specific basic conditions are shown in Table 1.

Table 1. Sample Basic Information

Tree Species Number	DBH (cm)	Sample Height (cm)	Density (g/cm^3)	Moisture Content (%)
Y1	17.43	70.8	0.607	45.99
Y2	20.82	71.6	0.686	56.06
Y3	33.63	75.6	0.584	60.45
Y4	20.72	84.2	0.594	51.23

The Arbotom nondestructive stress wave tester (RINNTECH, Heidelberg, Germany) was used, as shown in Fig. 2. The tester contains 12 sensors and analysis software system, which can measure the propagation time and propagation velocity of stress wave among sensors, generating the corresponding matrix reports. A 202-0 desktop dryer (YONG GUANG MING, Beijing, China) and Sanfeng electronic scale (INESA, Shanghai, China) were used to measure the moisture content of wood.

Fig. 2. Setup of nondestructive testing experiments of (a) healthy sample detection, (b) defective sample detection

Methods

Measurement of stress wave propagation velocity

(1) Measurement of stress wave propagation velocity in different direction angles. A longitudinal section of the test sample was selected, and sensors were placed 5cm away from the top of the sample, 6 sensors on each side. The distance between two adjacent sensors on the same side is 10 cm, and the direction angle between the contralateral sensors was represented by α. The sensor No.1- No.6 was the transmitter, and No. 7 - No. 12 were the receiver, as shown in Fig. 3(a). The sensors of No.1- No.6 were struck in sequence, and each sensor is tapped 5 to 8 times. The propagation velocity and time of stress wave in healthy log samples were obtained by Arbotom stress wave tester. The same longitudinal section was measured 3 times and averaged.

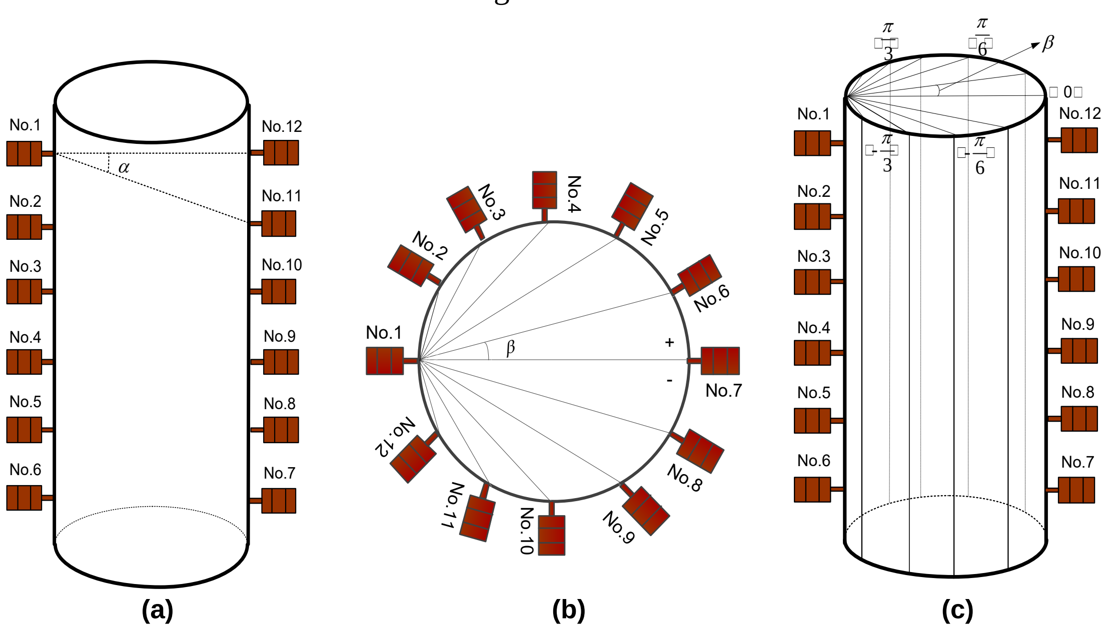

Fig. 3. Distribution of stress wave sensors in (a) different direction angles, (b) different longitudinal section angles, (c) longitudinal section with different directions

(2) Measurement of stress wave propagation velocity in different longitudinal section angles. A cross section was selected with different longitudinal sections of the test sample and place sensor No. 1 1m above the ground and sensor No. 12 at the other end of

the diameter at the same height, then, sensors were arranged at intervals of $\frac{\pi}{12}$ in positive and negative directions, as shown in Fig. 3(b). The sensor No.1 was the transmitter, and No. 2 - No. 12 were the receiver, the angle between adjacent sensors was denoted by β.

(3) Measurement of stress wave propagation velocity in longitudinal section with different directions. The larch logs were selected as test samples, and the sensor arrangement of the stress wave tester was shown in Fig. 3(c). Sensors No.1 - No.6 were used as the transmitting end, and No.7 - No.12 were the receiving end. The samples propagation velocities of the 11 longitudinal section stress wave in different directions were measured.

(4) Measurement of stress wave propagation velocity in defective logs. Circular hollow defects of 2.5 cm, 5 cm, 7.5 cm, and 10 cm in diameter were manually cut in the middle position of the larch logs, and the same experimental method was adopted for testing.

Imaging of internal defects in logs

Based on the established regression model of the stress wave propagation velocity and longitudinal section in different directions, the defect area was obtained by reconstruction of larch defect two-dimensional image (Huang *et al.* 2013; Liu *et al.* 2019). The steps are shown in Fig. 4.

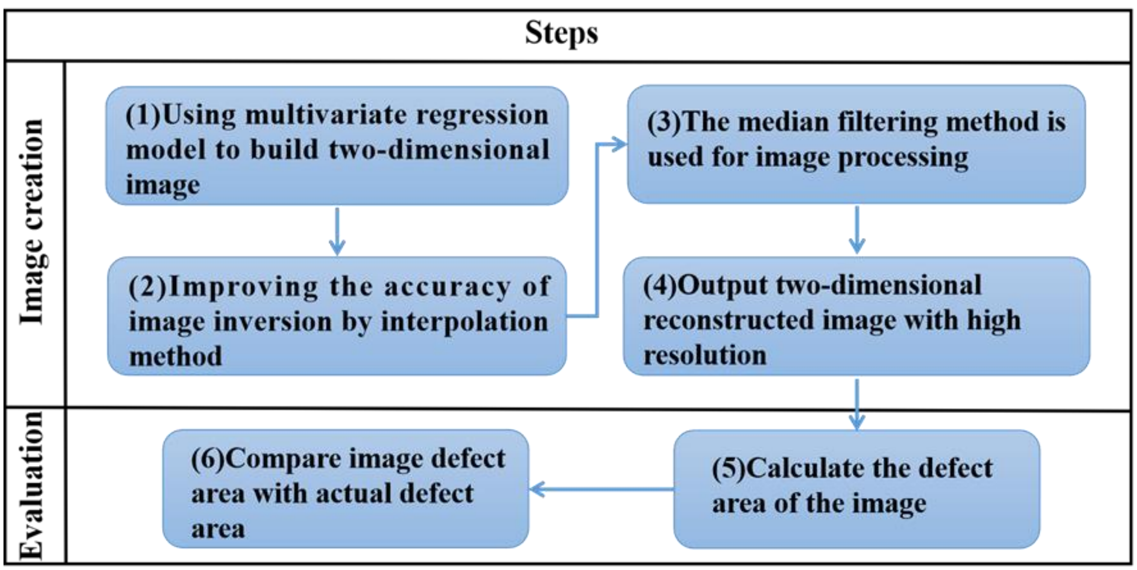

Fig. 4. Steps to internal defect imaging

Determination of moisture content

The variation of wood moisture content can have a great influence on the propagation velocity of stress wave (Baranski 2018; Gao *et al.* 2018). In order to reduce the influence of the change of sample moisture content, the sample was packaged during transportation, and it was transported back to the laboratory at an ambient temperature of 23 °C and air relative humidity of 54% for 48 h. The moisture content of the samples was measured after transportation. Reference was made to ISO 3130 (1975), a representative moisture content test piece with a thickness of 0.01 m was sawed at a distance of 0.24 m from the end of the sample, and the weight was regarded as the quality of the wet material of the log, which it was tested. The sample was then dried in a constant temperature oven at 103 ± 2 °C for about 24 h. The weight was taken out and recorded, and then returned to the oven for further drying. It is weighed every 4 h until the weight of the last two weights is constant, which is recorded as the absolute dry weight of the test piece, as illustrated in Fig. 5.

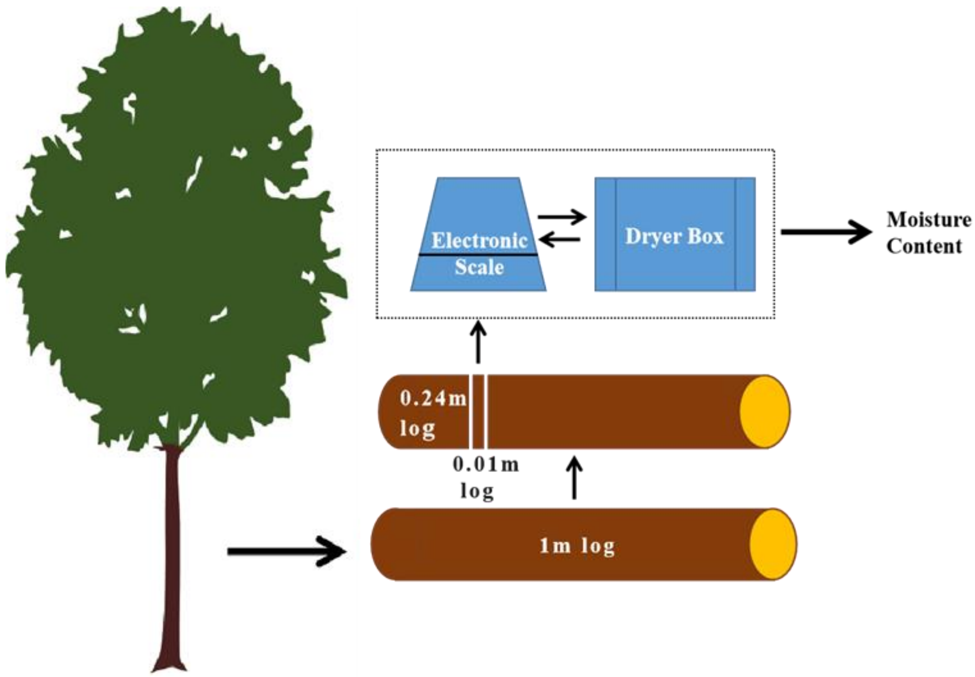

Fig. 5. Moisture content testing process

The formulas for calculating the moisture content of four samples are as follows:

$$M = \frac{m - m_0}{m_0} \times 100\% \tag{5}$$

where M is the moisture content of the sample(%), m is the quality of the test piece(g), and m_0 is the quality of the test piece when it is completely dry(g).

RESULTS AND DISCUSSION

An Arbotom stress wave nondestructive wood tester was used to measure the propagation velocity of stress wave in different direction angles, longitudinal section angle of Y1-Y4 logs. The relationship between the propagation velocity and the direction angles and the longitudinal section angles was obtained.

Analysis of the Propagation Velocity of Stress Wave in Different Direction Angles

When the longitudinal section angle was $\frac{\pi}{12}$, the propagation velocity of stress wave of different direction angles between the sensor No.1 and the sensor No.7- No.12 were measured on the healthy Y1-Y4 logs. The results are shown in Table 2.

The stress wave propagation velocities of the four healthy log samples in different direction angles are different. The higher the wood density was, the higher the propagation velocity was, but the variation law increased with the increase of the direction angles, and the propagation velocity in the horizontal direction was the smallest (Table 2). Using SPSS data analysis software, the data in Table 2 were plotted as scatter plots of direction angle and stress wave propagation velocity, and the curve was fitted according to the mathematical model ($y = ax^2 + b$) of Eq. 2, as shown in Fig. 6, where the abscissa x represents direction angle α, expressed in radians, and the longitudinal coordinate y represents the stress wave propagation velocity v. The results show that the coefficients of determination R^2 of the four samples were all above 0.83, and the significance P was less than 0.01, which indicates that the theoretical mathematical model of Eq. 2 had a good goodness of fit and was suitable for establishing the relationship between stress wave propagation velocity and direction angle of different tree species, which verified the correctness of the theoretical model.

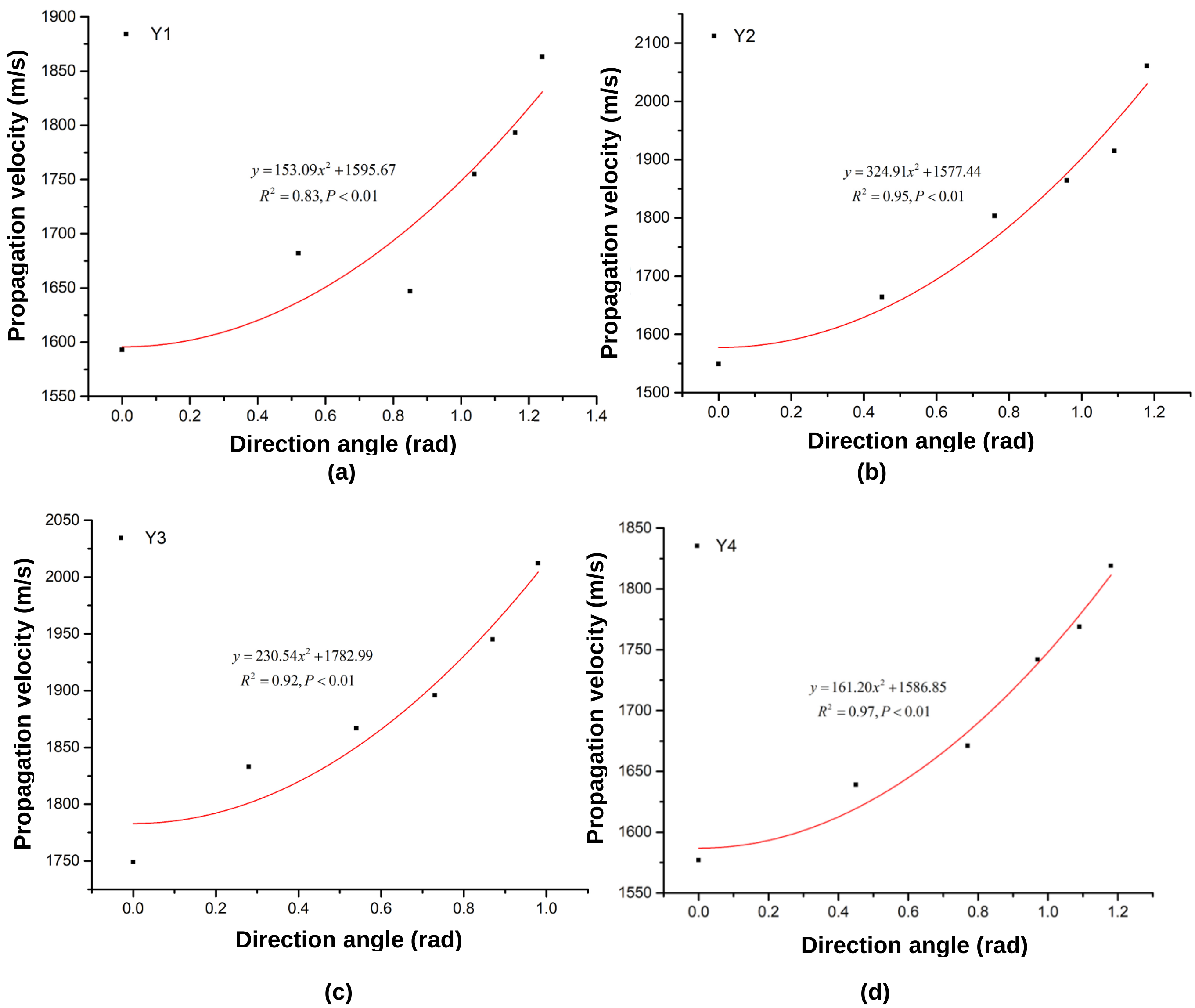

Fig. 6. Fitting curve of stress wave propagation velocity in different direction angles of healthy Y1-Y4 logs

Table 2. Stress Wave Propagation Velocities of Healthy Y1-Y4 Logs in Different Direction Angles

Tree Species	Propagation Velocity (m/s)					
	1-12	1-11	1-10	1-9	1-8	1-7
Y1	1593	1682	1647	1755	1793	1863
Y2	1549	1664	1803	1864	1915	2061
Y3	1749	1833	1867	1896	1945	2012
Y4	1577	1639	1671	1742	1769	1819

Analysis of the Propagation Velocity of Stress Wave in Different Longitudinal Section Angles

When the orientation angle was 0, the stress wave propagation velocities of four kinds of healthy log samples in different longitudinal section angles between No.1- No.12 sensors were measured. The results are shown in Table 3.

Table 3. Stress Wave Propagation Velocity in Different Longitudinal Section Angles of Healthy Y1-Y4 Logs

Tree Species	Propagation Velocity（m/s）										
	$-\frac{2\pi}{3}$	$-\frac{\pi}{3}$	$-\frac{\pi}{4}$	$-\frac{\pi}{6}$	$-\frac{\pi}{12}$	0	$\frac{\pi}{12}$	$\frac{\pi}{6}$	$\frac{\pi}{4}$	$\frac{\pi}{3}$	$\frac{2\pi}{3}$
Y1	1352	1455	1592	1674	1607	1690	1682	1603	1568	1489	1294
Y2	1115	1204	1407	1519	1553	1614	1549	1489	1386	1294	1103
Y3	1483	1634	1705	1764	1795	1764	1749	1753	1712	1604	1507
Y4	1320	1432	1503	1594	1574	1593	1577	1537	1522	1428	1407

The data in Table 3 were plotted as scatter points and fitted with curves, and the corresponding fitting equation was given, as shown in Fig. 7. The longitudinal section angle β is represented by abscissa x, the corresponding stress wave propagation velocity v is represented by longitudinal coordinate y, and the trend of stress wave propagation velocity in four samples in different longitudinal section angles are represented by four graphs, that is, the stress wave propagation velocity decreases with the increase of longitudinal section angles and the radial propagation velocity is the largest. The overall trend is a parabola downward from the opening, which is symmetrical about 0. The one-dimensional quadratic function relation $y = ax^2 + b + c$ is satisfied by analysis, $b \approx 0$, a depending on the physical and mechanical parameters of the sample (elastic modulus, density and moisture content, *etc.*), in accordance with the mathematical model of the theoretical model (Eq. 3), and the correlation coefficients R^2 are above 0.92, the significance P is less than 0.01, and the theoretical and experimental mathematical models have a significant goodness of fit.

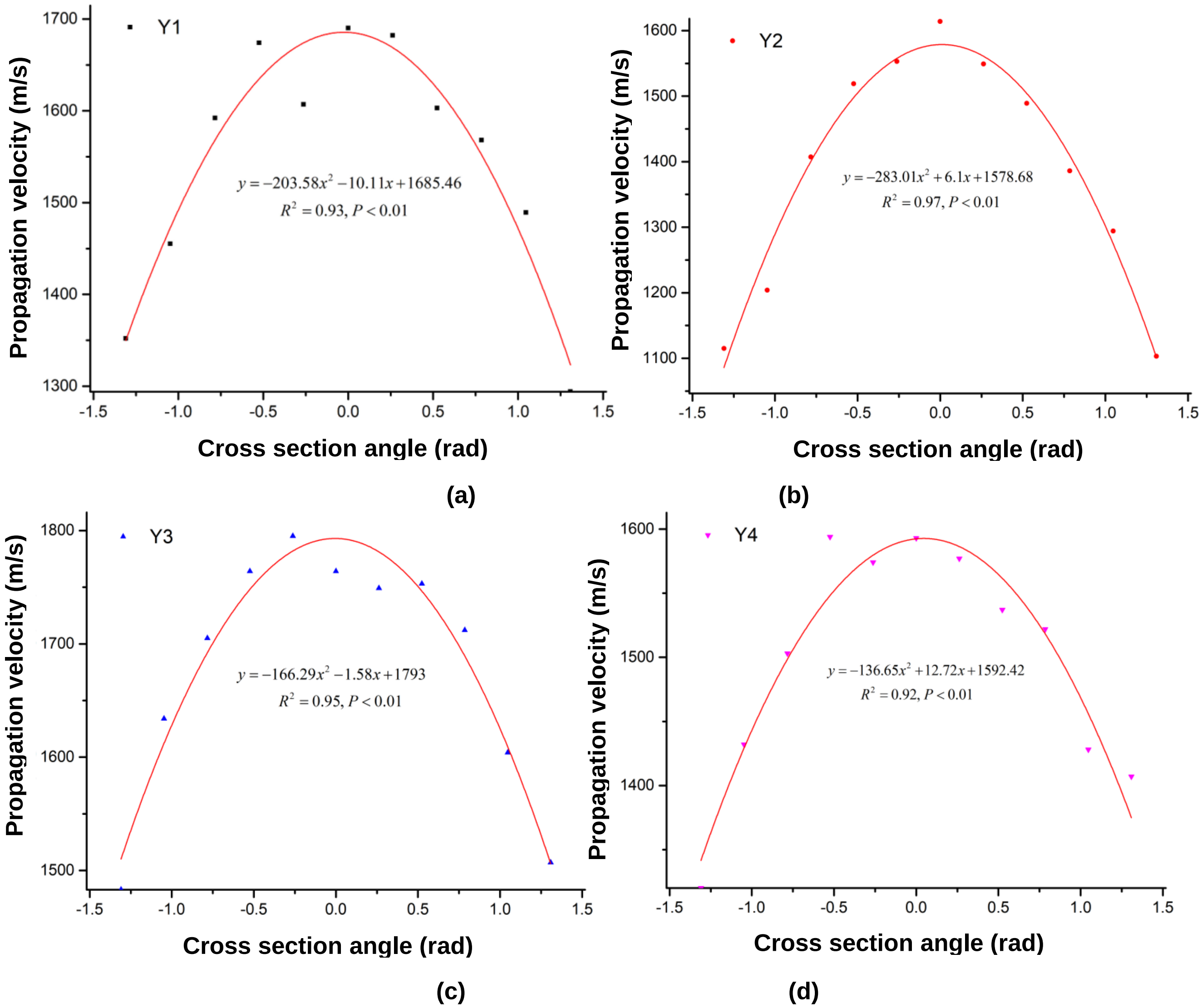

Fig. 7. Fitting curve of stress wave propagation velocity in different longitudinal section angles of healthy Y1-Y4 logs

Analysis of the Propagation Velocity of Stress Wave in Longitudinal Section with Different Direction Angles

The larch logs were selected as the test sample, and the stress wave propagation velocities of longitudinal sections with different directions were measured by experiments (Fig. 3(C)). The cftool toolbox in Matlab software drawing function was used, combined with the mathematical model ($z=Ax^2-By^2+Cx^2y^2-Dx^2y^4+E$) of Eq. 4 to realize the three-dimensional spatial diagram drawing, as shown in Fig. 8. The x coordinate represents the direction angle (downward is positive, upward is negative), the y coordinate represents the intersection angle (clockwise is negative, counterclockwise is positive), and the z coordinate indicates the stress wave velocity. The three-dimensional surface map shows that the interaction between the direction angle and longitudinal section angle have a great influence on the propagation of the stress wave, which the propagation velocity of the stress wave propagates symmetrically with the direction angle and the longitudinal section angle.

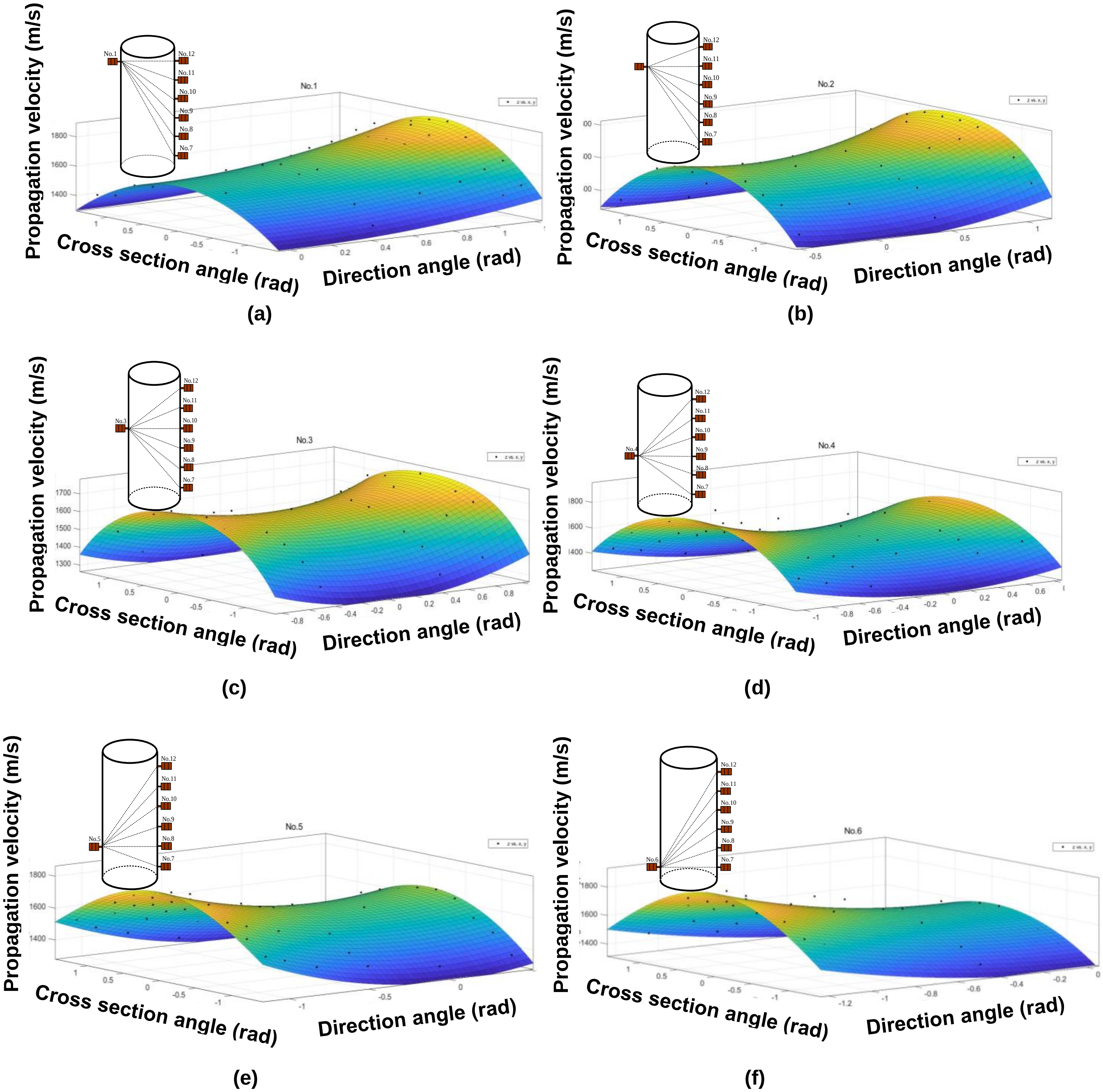

Fig. 8. Stress wave velocity fitting surface of longitudinal section of healthy larch in different directions

As shown in Table 4, the coefficients of determination R^2 of the fitting equations of the continuous surfaces in the regression analysis were all above 0.92, and the significance P was less than 0.01. This indicated that the regression models of the established continuous surfaces had good goodness of fit. The propagation law of the well-reacted stress wave in the longitudinal section of the larch in different directions was very consistent with the theoretical mathematical model (Eq. 4) established in this paper. From the fitting results, there was a difference between the corresponding coefficients of the fitting equations, which was related to the water content change and measurement error of the larch logs. When the sensor No. 3 was used as the transmitting end, the correlation coefficient of the fitting equation (z = 109.2x^2 - 182.1y^2 + 36.78x^2y^2 - 34.76x^2y^4 + 1627) was higher than No. 4 (R^2 = 0.97), the root mean square error was small (*RMSE* = 17.81), and the fitting degree of the equation was high. Therefore, the regression equation obtained by the sensor No. 3 was selected as the continuous multiple regression model of a surface.

Table 4. Fitting Equation for Longitudinal Section of Healthy Larch in Different Directions

Sensor Number	Fitting Equation $z=Ax^2-By^2+Cx^2y^2-Dx^2y^4+E$	Correlation Coefficient R^2	*P*	Root Mean Square Error *RMSE*
No 1	$z=166.3x^2-144.5y^2+22.88x^2y^2-30.11x^2y^4+1599$	0.95	<0.01	27.77
No 2	$z=137.5x^2-170.5y^2+44.54x^2y^2-28.3x^2y^4+1622$	0.97	<0.01	20.92
No 3	$z=109.2x^2-182.1y^2+36.78x^2y^2-34.76x^2y^4+1627$	0.97	<0.01	17.81
No 4	$z=199.5x^2-158.3y^2+12.92x^2y^2-15.89x^2y^4+1598$	0.92	<0.01	48.28
No 5	$z=160.1x^2-168.2y^2+49.77x^2y^2-22.29x^2y^4+1616$	0.96	<0.01	24.96
No 6	$z=188.1x^2-153.2y^2+6.92x^2y^2-17.16x^2y^4+1608$	0.96	<0.01	28.29

Comparison of Stress Wave Propagation Velocity between Healthy Logs and Defective Logs in Longitudinal Section with Different Directions

When the longitudinal section angle was 0, the propagation velocity of stress wave in different directions was measured for healthy larch log and defective larch log with diameter of 7.5 cm, and using SPSS to draw the change trend of stress wave propagation. Fig. 9 shows the trend of stress wave propagation velocity of healthy and defective log with sensor No. 3 as the transmitter and sensor No. 7-12 as the receiver. The value of velocity for the point 3-9 for defective larch log is lower than that of the healthy log.

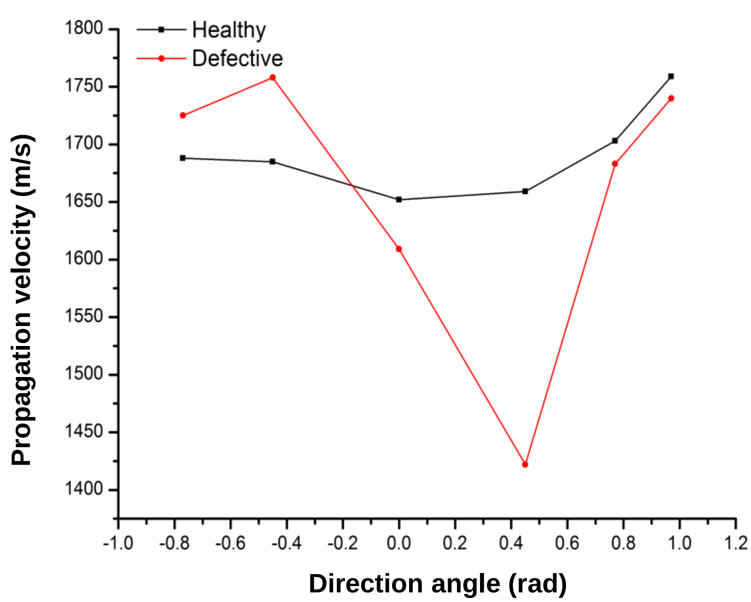

Fig. 9. Stress wave propagation velocity trends in healthy and defective larch logs

.

Table 5. Stress Wave Propagation Velocities in Longitudinal Sections of Healthy Larch and Defective Larch (7.5 cm) with Different Directions

		$-\frac{2\pi}{3}$	$-\frac{\pi}{6}$	$-\frac{\pi}{4}$	$-\frac{\pi}{6}$	$-\frac{\pi}{12}$	0	$\frac{\pi}{12}$	$\frac{\pi}{6}$	$\frac{\pi}{4}$	$\frac{\pi}{3}$	$\frac{2\pi}{3}$
3-12	v1 (m/s)	1403	1517	1589	1653	1701	1688	1693	1655	1614	1513	1421
	v2 (m/s)	1405	1535	1610	1647	1680	1725	1654	1642	1632	1530	1412
	Δv (%)	0.14	1.17	1.30	0.36	1.25	2.14	2.36	0.79	1.10	1.11	0.64
3-11	v1 (m/s)	1366	1483	1560	1607	1624	1685	1654	1613	1573	1507	1349
	v2 (m/s)	1357	1483	1547	1539	1639	1758	1663	1608	1583	1478	1365
	Δv (%)	0.66	0	0.84	4.41	0.92	4.15	0.54	0.31	0.63	1.96	1.17
3-10	v1 (m/s)	1301	1419	1503	1542	1599	1652	1601	1567	1512	1437	1286
	v2 (m/s)	1289	1427	1503	1547	1567	1609	1572	1559	1521	1422	1308
	Δv (%)	0.93	0.56	0	0.32	2.04	2.67	1.84	0.51	0.59	1.05	1.68
3-9	v1 (m/s)	1349	1485	1547	1593	1642	1659	1603	1604	1549	1492	1323
	v2 (m/s)	1344	1470	1556	1468	1480	1422	1468	1477	1559	1486	1363
	Δv (%)	0.37	1.02	0.58	**8.51**	**10.95**	**16.67**	**9.2**	**8.6**	0.64	0.4	2.93
3-8	v1 (m/s)	1415	1503	1607	1646	1663	1703	1675	1650	1613	1524	1409
	v2 (m/s)	1390	1512	1623	1683	1652	1683	1660	1632	1607	1531	1412
	Δv (%)	1.8	0.6	1	2.2	0.6	1.19	0.9	1.1	0.37	0.46	0.21
3-7	v1 (m/s)	1460	1566	1663	1702	1685	1759	1719	1703	1685	1586	1483
	v2 (m/s)	1448	1569	1669	1715	1705	1740	1725	1698	1642	1602	1475
	Δv (%)	0.83	0.19	0.36	0.7	1.17	1.09	0.35	0.29	2.62	1	0.54

To study the stress wave propagation velocity in healthy and defect areas, 11 longitudinal sections of larch logs with defects were measured at $\pm\frac{\pi}{12}$, $\pm\frac{\pi}{6}$, $\pm\frac{\pi}{4}$, $\pm\frac{\pi}{3}$ and $\pm\frac{2\pi}{3}$. The stress wave passed through the void defect when the longitudinal angle was 0, $\pm\frac{\pi}{12}$, $\pm\frac{\pi}{6}$. Table 5 shows that the stress wave propagation velocity changed more after passing through the defect than in the healthy area. According to Wang *et al.* (2004), when the measured stress wave propagation velocity on a certain propagation path of a cross section of a tree was greater than 10% of its reference value, the path could be regarded as passing through the defect area. In this paper, the detection of larch showed it is considered defective when the propagation velocity of stress wave is more than 8.5% different from the normal value on a certain path of longitudinal section. The parameters v_1 and v_2 indicate the propagation velocity of the stress wave in the longitudinal section of the healthy and hollow larch logs, respectively, in different angles($\Delta v = \left|\frac{v_1 - v_2}{v_1}\right|$).

Detection of Internal Defects of Logs Using Stress Wave Propagation Velocity Model

According to the steps of image creation (Fig. 4), the two-dimensional imaging of the defective logs was realized by using programming in Python. Because the propagation velocity of stress wave was lower than the normal value in defect position, the imaging method was used after testing.

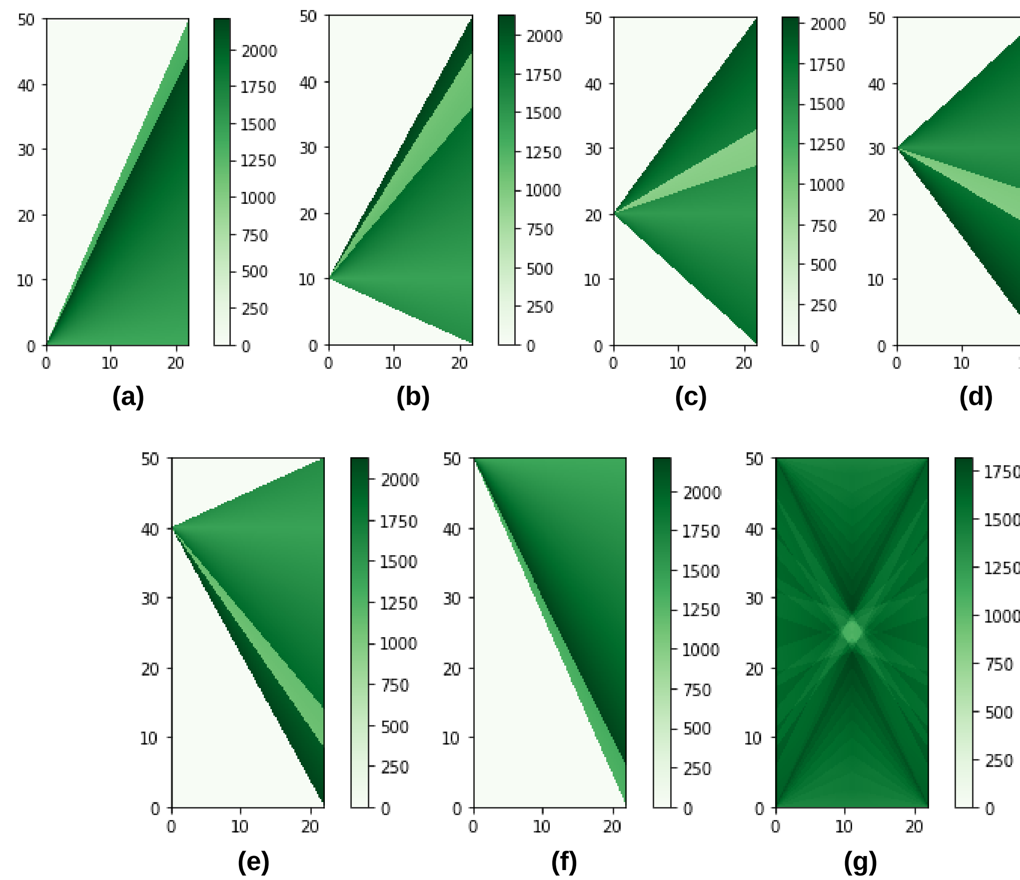

Fig. 10. Diagram of two-dimensional imaging process

The results calculated by theoretical model were used as reference value in this experiment. If the values differ by the measured value and the reference more than 8.5%, the tree has defects in the propagation path. The two-dimensional image of a defect (2.5 cm) with an angle of 0 in the section of larch sample is shown by Fig. 10. The y-axes (0, 10, 20, ..., and 50) represent the height position of the sensors on the same longitudinal section; the light color is through the defect area and through the superposition to form the defect diagram (Fig. 10g).

The analysis found that the imaging results were good, but there were still light-colored unclear areas. To improve the image resolution, the image was optimized, and a two-dimensional image of voids of different diameters as shown in Fig. 11.

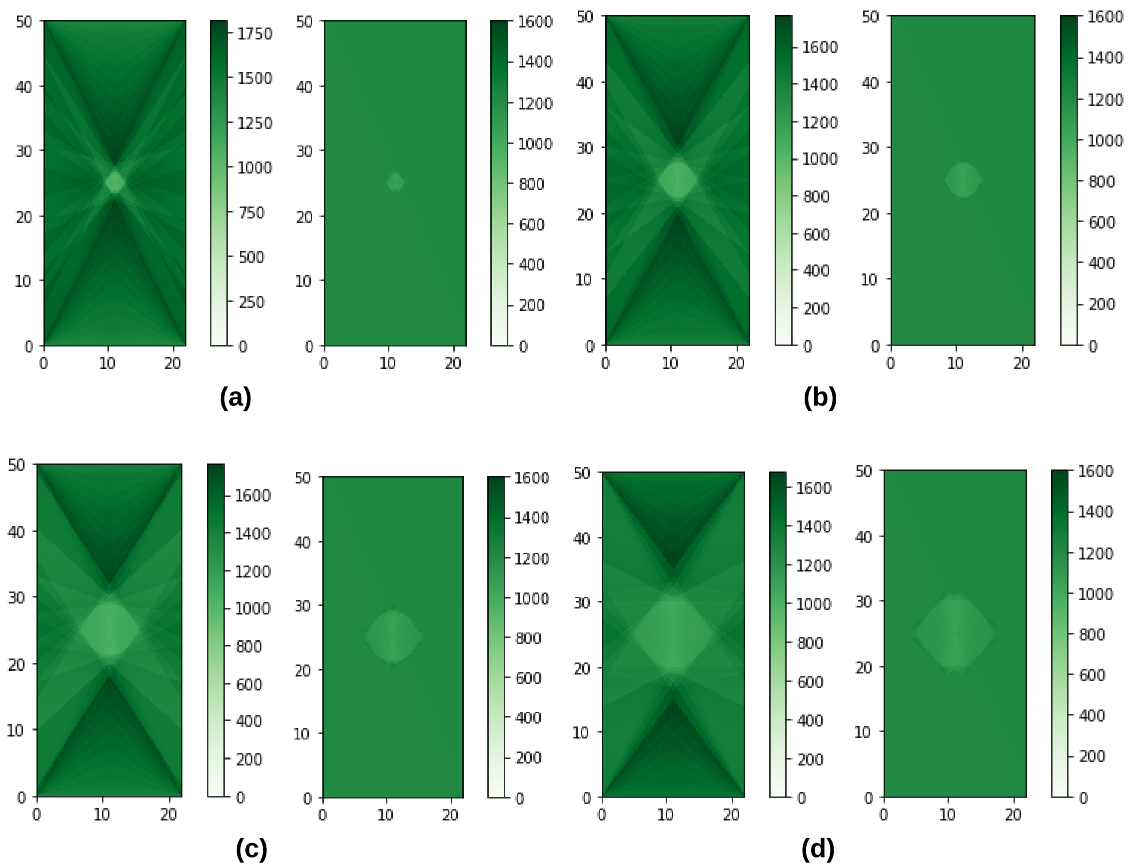

Fig. 11. Imaging of void defects for (a) 2.5cm diameter, (b) 5 cm diameter, (c) 7.5 cm diameter, (d) 10 cm diameter

In order to analyze the accuracy of the two-dimensional imaging effect in the detection of void defects, the image fitting degree and error rate are set as the indicators, which are expressed by T and λ, respectively (Riggio *et al.* 2015). The image fitting degree T is defined as the ratio of the actual defect area to the defect area of the reconstructed image, that is, $T\,(\%) = (S_z / S_j) \times 100$. The error rate reflects the degree of deviation between the reconstructed defect area and the actual defect area, that is, $\lambda = \frac{|S_j - S_z|}{S_z} \times 100\%$. S_j is the reconstructed defect area and S_z is the actual defect area.

Table 5. Stress Wave Propagation Velocities in Longitudinal Sections of Healthy Larch and Defective Larch (7.5 cm) with Different Directions

Cavity Diameter (cm)	Actual Defect Area S_z (cm^2)	Reconstruction Defect Area S_j (cm^2)	Image Fitness (%)	Error Rate (%)
2.5	4.91	5.21	94.24	6.11
5	19.63	20.92	93.83	6.57
7.5	44.3	48.18	91.95	8.76
10	78.5	85.28	92.04	8.64

Comparing the reconstructed defect area with the actual defect area of wood, the fitting degree and error rate of the reconstructed image were 94.24%, 93.83%, 91.95%, 92.04% and 6.11%, 6.57%, 8.76%, 8.64%, respectively. The imaging effect was not affected by the size of the defect cavity. It was close to the measured defect area, and it had a good detection effect (Table 5). The defect sample can also be subjected to two-dimensional imaging with direction angles of $\pm\frac{\pi}{12}$, $\pm\frac{\pi}{6}$, $\pm\frac{\pi}{4}$, $\pm\frac{\pi}{3}$ and $\pm\frac{2\pi}{3}$, so that the position of the defect and the volume of the defect can be detected more accurately.

The propagation velocity of stress wave increase with the increase of direction angle α, and the horizontal velocity was the smallest, which was a quadratic function curve. The propagation velocity of the stress wave varied with the longitudinal section angle β, the angle increase and the radial propagation velocity was the largest, for which the overall trend was a parabola with an opening downward. The reason is that wood is an anisotropic material. A stress wave, as an elastic mechanical wave, will have different propagation velocity in different directions of the same tree species when it propagates in wood. When the tree rings were uniform, the material was dense and the texture was straight, the cut material was uniform, and the tubular cells were arranged neatly and straight, which was beneficial to the propagation of elastic waves, that is, the stress wave propagated fastest in the direction of the same tree species, and the radial propagation velocity under the transverse stripes was greater than the chord propagation velocity.

In the healthy part of trees, the propagation velocity of stress wave varies with the direction angle and longitudinal section angle, which satisfies the propagation velocity model of healthy trees. A stress wave always propagates along the shortest path according to the propagation mechanism of stress wave and Fermat Principle. However, propagation time of stress wave is prolonged when stress wave propagates to defective areas, and the propagation velocity is significantly decreased, which no longer conforms to the propagation velocity model under normal conditions. The two-dimensional imaging of cavity defects of 2.5 cm, 5 cm, 7.5 cm and 10 cm is realized based on the established stress wave propagation velocity model of longitudinal section in different directions. This method can detect the location and size of the internal defects of the wood more accurately compared with the four-way cross-detection method of tree interior defect using propagation velocity model. It also provides theoretical and experimental basis for further realization of three-dimensional imaging.

CONCLUSIONS

1. The variation of stress wave propagation velocity in the longitudinal section of trees with different direction angles was analyzed, the corresponding theoretical model of propagation velocity was established. The stress wave propagation velocity model satisfied the function formula $v_r+v_r(1-v_r/v_l)\alpha^2$ in different direction angles α and the function formula $(1-0.2\beta^2)v_R$ in different longitudinal section angles β. The two models were integrated to obtain velocity propagation model $v(\alpha,\beta)=A\alpha^2-B\beta^2+C\alpha^2\beta^2-D\alpha^2\beta^4+K$.
2. The non-destructive testing of stress wave was completed for different tree species. The propagation velocity model of stress wave in longitudinal section of birch, ashtree, elm, and larch in different angles was established. The test results showed that the stress wave had the same law in different tree species. In the same longitudinal section, the propagation velocity of the stress wave increased with the increase of the direction angle, and the velocity of the horizontal direction was the smallest. In the same direction, the propagation velocity of the stress wave increased with the increase of the longitudinal section angle, and the velocity of the radial was maximum. The regression analysis results showed that the regression models established by different tree species had good goodness of fit, which was in good agreement with the theoretical mathematical model established in this paper.
3. Based on the established propagation velocity model of stress waves in trees, defect detection of larch logs containing voids was finished. Since the stress wave propagation velocity through the defect location was significantly lower than the normal value, the experiment was designed to complete the detection test of the larch containing void, and a two-dimensional imaging method based on the multivariate regression model was established. The position and size of the internal defects of the tree can be defected accurately, and the fit of the reconstructed image was above 94.24%. The imaging effect was not affected by the size of the defect cavity, which laid a foundation for the future three-dimensional imaging using stress waves.

ACKNOWLEDGMENTS

The authors are grateful for the support of the National Forestry Public Welfare Industry Scientific Research Project (Grant No.201304502), the Higher Education Teaching Reform Project in Heilongjiang Province (Grant No.SJGY20180433).

REFERENCES CITED

Baranski, J. (2018). "Moisture content during and after high-and normal-temperature drying processes of wood," *Drying Technology* 36(6), 751-761. DOI: 10.1080/07373937.2017.1355319

Bucur, V. (2005). "Ultrasonic techniques for nondestructive testing of standing trees," *Ultrasonics* 43(4), 237-239. DOI: 10.1016/j.ultras.2004.06.008

Chang, L., Dai, J., and Qian, W. (2016). "Nondestructive testing of internal defect of ancient architecture," *Journal of Beijing University of Technology* 42(6), 886-892.

Du, X. C., Feng, H. L., Hu, M. Y., Fang, Y. M., and Chen, S. Y. (2018a). "Three-dimensional stress wave imaging of wood internal defects using TKriging method," *Computers and Electronics in Agriculture* 148, 63-71. DOI: 10.1016 /j.compag.2018.03.005

Du, X., Li, J., Feng, H., and Chen, S. (2018b). "Image reconstruction of internal defects in wood based on segmented propagation rays of stress waves," *Applied Sciences* 8(10), 1778. DOI: 10.3390/app8101778

Du, X., Li, S., Li, G., Feng, H., and Chen, S. (2015). "Stress wave tomography of wood internal defects using ellipse-based spatial interpolation and velocity compensation," *BioResources* 10(3), 3948-3962. DOI: 10.15376/biores.10.3.3948-3962

Feng, H., Li, G., Fu, S., and Wang, X. (2014). "Tomographic image reconstruction using an interpolation method for tree decay detection," *BioResources* 9(2), 3248-3263. DOI: 10.15376/biores.9.2.3248-3263

Gao, X., Li, Q., Cheng, W., Han, G., and Xuan, L. (2018). "Effects of moisture content, wood species, and form of raw materials on fiber morphology and mechanical properties of wood fiber-HDPE composites," *Polymer Composites* 39(9), 3236-3246. DOI: 10.1002/pc.24336

Huan, Z., Jiao, Z., Li, G., and Wu, X. (2018). "Velocity error correction based tomographic imaging for stress wave nondestructive evaluation of wood," *BioResources* 13(2), 2530-2545. DOI: 10.15376/biores.13.2.2530-2545

Huang, Y. H., Chung, C. H., Wu, M. L., and Lin, C. J. (2013). "Stress wave tomogram and wood density profile in a royal palm tree: A case study," *Taiwan Journal of Forest Science* 28(3), 129-144.

ISO 3130. (1975). "Wood – Determination of moisture content for physical and mechanical tests," International Organization for Standardization, Geneva, Switzerland.

Liang, S., and Fu, F. (2012). "Strength loss and hazard assessment of Euphrates poplar using stress wave tomography," *Wood and Fiber Science* 44(1), 54-62.

Liang, S., and Fu, F. (2014). "Effect of sensor number and distribution on accuracy rate of wood defect detection with stress wave tomography," *Wood Research (Bratislava)* 59(4), 521-532.

Liao, C., Zhang, H., Song, X., Chen, T., and Huang, S. (2017). "The screening method of the internal defects in wood members of the ancient architectures by hammering sound," *BioResources* 12(2), 2711-2720. DOI: 10.15376/biores.12.2.2711-2720

Lin, C., Chang, T., Juan, M., Lin, T., Tseng, C., Wang, Y., and Tsai, M. (2011). "Stress wave tomography for the quantification of artificial hole detection in camphor trees (*Cinnamomum camphora*)," *Taiwan Journal of Forest Science* 26(1), 17-32.

Liu, L., and Li, G. (2018). "Acoustic tomography based on hybrid wave propagation model for tree decay detection," *Computers and Electronics in Agriculture* 151, 276-285. DOI: 10.1016/j.compag.2018.06.020

Liu, W., Xie, W., Dang, Y., Yan, C., and Tang, A. (2019). "Image reconstruction modeling, simulation and experimental study on wood fibrous paper," *Journal of Natural Fibers* 1-14. DOI: 10.1080/15440478.2019.1585309

Mascia, N. T., Nicolas, E. A., Cammpinas, S., and Todeschini, B. R. (2011). "Comparison between Tsai-Wu failure criterion and Hankinson's formula for tension in wood," *Wood Research* 56(4), 499-510.

Rabe, C., Ferner, D., Fink, S., and Schwarze, F. W. M. R. (2004). "Detection of decay in trees with stress waves and interpretation of acoustic tomograms," *Arboricultural*

Journal 28(1-2), 3-19. DOI: 10.1080/03071375.2004.9747399
Riggio, M., Sandak, J., and Franke, S. (2015). "Application of imaging techniques for detection of defects, damage and decay in timber structures on-site," *Construction and Building Materials* 101, 1241-1252. DOI: 10.1016/j.conbuildmat.2015.06.065
Ross, R. J., Brashaw, B. K., and Pellerin, R. F. (1998). "Nondestructive evaluation of wood," *Forest Products Journal* 48(1), 14.
Romano, A. J., Bucaro, J. A., and Dey, S. (2008). "Defect detection and localization in orthotropic wood slabs by inversion of dynamic surface displacements," *The Journal of the Acoustical Society of America* 124(2), 918-925. DOI: 10.1121/1.2945706
Simic, K., Gendvilas, V., O'Reilly, C., and Harte, A. M. (2019). "Predicting structural timber grade-determining properties using acoustic and density measurements on young Sitka spruce trees and logs," *Holzforschung* 73(2), 139-149. DOI: 10.1515/hf-2018-0073
Wang, X., Ross, R. J., McClellan, M., Barbour, R. J., Erickson, J. R., Forsman, J. W., and McGinnis, G. D. (2001). "Nondestructive evaluation of standing trees with a stress wave method," *Wood and Fiber Science* 33(4), 522-533.
Wang, X., Divos, F., Pilon, C., Brashaw, B. K., Ross, R. J., and Pellerin, R. F. (2004). *Assessment of Decay in Standing Timber Using Stress Wave Timing Nondestructive Evaluation Tools* (Report No. FPL-GTR-147), U.S. Department of Agriculture, Forest Products Laboratory, Madison, WI.
Wang, L., Wang, Y., and Xu, H. (2011). "Effects of tangential angles on stress wave propagation velocities in logs cross sections," *Scientia Silvae Sinicae* 47(8), 139-142.
Weng, X., Li, G., Feng, H., Du Xiaochen, and Chen, F. (2016). "Stress wave propagation velocity model in RL plane of standing trees," *Scientia Silvae Sinicae* 52(7), 104-112.
Watanabe, K., Saito, Y., Avramidis, S., and Shida, S. (2008). "Non-destructive measurement of moisture distribution in wood during drying using digital X-ray microscopy," *Drying Technology* 26(5), 590-595. DOI: 10.1080/07373930801944796
Xu, F., Wang, X., Thomas, E., Liu, Y., Brashaw, B. K., and Ross, R. J. (2018). "Defect detection and quality assessment of hardwood logs: Part 1—Acoustic impact test and wavelet analysis," *Wood and Fiber Science* 50 (3), 291-309. DOI: 10.22382/wfs-2018-029
Yang, X., and Wang, L. (2005). "Study on the propagation theories of stress wave in log," *Scientia Silvae Sinicae* 41(5), 132-138.
Yue, X., Wang, L., Wacker, J. P., and Zhu, Z. (2019). "Electric resistance tomography and stress wave tomography for decay detection in trees—A comparison study," *PeerJ* 7, e6444. DOI: 10.7717/peerj.6444

Article submitted: July 23, 2019; Peer review completed: August 26, 2019; Revised version received and accepted: September 19, 2019; Published: September 24, 2019.
DOI: 10.15376/biores.14.4.8904-8922